Structural Engineering and Mechanics, *Vol. 67, No. 6 (2018) 603-616*
DOI: https://doi.org/10.12989/sem.2018.67.6.603

Highly accurate family of time integration method

Mohammad Rezaiee-Pajand*, S.A.H. Esfehani and Mahdi Karimi-Rad

Department of Civil Engineering, Ferdowsi university of Mashhad, Mashhad, Iran

(Received October 26, 2017, Revised May 13, 2018, Accepted July 4, 2018)

Abstract. In this study, the acceleration vector in each time step is assumed to be a mth order time polynomial. By using the initial conditions, satisfying the equation of motion at both ends of the time step and minimizing the square of the residual vector, the m+3 unknown coefficients are determined. The order of accuracy for this approach is m+1, and it has a very low dispersion error. Moreover, the period error of the new technique is almost zero, and it is considerably smaller than the members of the Newmark method. The proposed scheme has an appropriate domain of stability, which is greater than that of the central difference and linear acceleration techniques. The numerical tests highlight the improved performance of the new algorithm over the fourth-order Runge-Kutta, central difference, linear and average acceleration methods.

Keywords: high accuracy; time integration scheme; nonlinear analysis; period error; stability

1. Introduction

Dynamic time integration methods are extensively used for structural dynamic analysis. To find this solution at time t, the time interval between 0 and t is subdivided into n time intervals Δt_j. Then, instead of satisfying the equation of motion at any time t, dynamic equilibrium is usually satisfied only at discrete time points. Furthermore, the variation of acceleration, velocity, and displacement within each time step is assumed to follow a special pattern (Park 1977, Felippa and Park 1979, Paz and Leigh 1985, Dokainish and Subbaraj 1989, Chopra 2007, Chang 2014). In some algorithms of the nonlinear analysis, the tangent stiffness matrix is computed at the beginning of each time step and the solution at the end of the step is determined based on this matrix (Paz and Leigh 1985, Mansur *et al.* 2000, Bathe 2006, Chopra 2007).

Time integration methods are categorized into two groups of explicit and implicit. In the explicit methods, the unknown solution at the end of a time step is explicitly determined based on the preceding responses (Hahn 1991, Chung and Lee 1994, Hulbert and Chung 1996, Zhai 1996, Pezeshk and Camp 1999, Chang and Liao 2005, Chang 2009, 2010, Rezaiee-Pajand and Hashemian 2016, Rezaiee-Pajand *et al.* 2017).

Two of the most popular explicit algorithms are the central difference and second-order Runge-Kutta (RK2) methods. In the implicit time integration schemes, the solution at the end of time step is determined by solving a system of algebraic equations involving both the current and following states of the structure (Alamatian 2013). Among the implicit techniques, the Newmark scheme is probably the most widely used implicit algorithm (Paz and Leigh 1985, Dokainish and Subbaraj 1989, Chopra 2007). Predictor-corrector methods which combine explicit and implicit schemes are also interesting approaches in structural dynamics. In these techniques, the responses are approximated by an explicit algorithm. Then, an implicit method is deployed to modify the obtained approximate responses (Kuo and Yau 2011, Rezaiee-Pajand and Hashemian 2016). Verma *et al.* (2015) assessed the performance of four numerical methods, namely, Central difference method, Operator splitting algorithm (Wu *et al.* 2006), Rosenbrock based technique (Bursi *et al.* 2008) and CR-integration method (Chen and Ricles 2008). These methods are widely used for real-time hybrid testing (RTHT).

Stability and accuracy are two important issues in the dynamic analysis. In the stability view point, there are two groups in time integration schemes. The first one contains conditionally stable algorithms in which the time step should be selected smaller than a specific value in order to instability does not occur. The second group contains unconditionally stable tactics in which instability never happens regardless of the time step size (Chen *et al.* 2009, Chang 2016, Tang and Lou 2017, Nguyen *et al.* 2017, Chang *et al.* 2017, Zheng *et al.* 2017). Among conditionally stable techniques, the linear acceleration and central difference methods have an acceptable region of stability (Subbaraj and Dokainish 1989, Chopra 2007, Kuo and Yau 2011, Yin 2013). The orders of accuracy, numerical dissipation and numerical dispersion are three significant factors for evaluating the accuracy of a scheme (Kuo *et al.* 2012, Chang 2015, Rezaiee-Pajand and Hashemian 2015, 2016). Based on the generalized-α scheme, Kolay and Ricles (2014) formulated an unconditionally stable algorithm for linear elastic and stiffness softening-type nonlinear systems. The amount of numerical damping was controlled by a single parameter. Chang (2014) presented a new family of unconditionally stable integration methods for structural dynamics. His method has the favorable

*Corresponding author, Professor
E-mail: rezaiee@um.ac.ir

ISSN: 1225-4568 (Print), 1598-6217 (Online)

numerical dissipation properties that can be continuously controlled. In addition, Chang *et al.* (2015) developed a new family of structure-dependent integration methods, which can eliminate unimportant high-frequency responses.

Wang and Au (2008) introduced two new types of integration methods based on Chebyshev polynomial of the first kind for dynamic response analysis of structures, namely the integral formula method (IFM) and the homogenized initial system method (HISM). Time integration algorithms can be constructed by using several frameworks such as finite difference methods, Hamilton's principle, Hamilton's law and weighted residual approaches. Fung (1999) developed a high-order accurate weighted residual scheme for dynamic analysis. Ghassemieh *et al.* (2016) proposed a weighted residual time integration technique, in which a second-order polynomial in time is deployed for approximating the acceleration vector. Furthermore, some researchers have proposed several methods for linear and nonlinear systems with the second order of accuracy (Bathe 2007, Liu *et al.* 2013, Rezaiee-Pajand and Karimi-Rad 2016, 2017, 2017; Mohammadzadeh *et al.* 2017, 2017, Chang 2018). Rezaiee-Pajand and Karimi-Rad (2016) suggested their technique based on Taylor series expansion. The stability of the scheme is controlled by two parameters. Based on a predictor-corrector approach, another technique was proposed, which can remove the spurious high-frequency components of the numerical responses (Rezaiee-Pajand and Karimi-Rad 2017). Bathe (2007) achieved a stable second-order accuracy procedure by conserving energy and momentum in nonlinear dynamics. In another event, Wen *et al.* (2014) introduced a novel method for linear systems, which has a limited order of accuracy. This was an explicit numerical integration scheme with three parameters utilizing periodic septuple B-spline interpolation polynomial functions. This technique was formulated for a single degree of freedom system, and then it was generalized for a multi degree of freedom one. Wen *et al.* (2017) proposed a multi sub-steps scheme for linear system. Their technique has a low order of accuracy. It was composed of three-time sub-steps. The trapezoidal rule and Houbolt method were employed in the first and third sub-steps, respectively. Moreover, in the second sub-step, the three-point Euler backward was applied. Bathe and Baig (2005) suggested a composite single step direct time integration technique. Klarmann and Wagner (2015) investigated the behavior of such methods in linear and nonlinear problems. Numerical instability is one of the most crucial difficulties in the nonlinear dynamic analysis. In this case, a very small time step should be utilized for the analysis. Several studies have been developed to overcome this kind of difficulty (Chang 2004, Rio *et al.* 2005, Chang 2007, Rezaiee-Pajand and Alamatian 2008).

In this paper, a new time integration method is proposed in which a *m*th order polynomial is used to approximate the acceleration vector. Author's formulations are presented for both linear and nonlinear dynamic analysis. The amplification matrix and region of stability for the suggested approach are determined. In addition, the orders of accuracy, numerical dissipation and numerical dispersion of the new technique are measured and compared to the other schemes. Several linear and nonlinear problems are solved by using the presented algorithm, and the results are compared with those of the Newmark, central difference and Runge-Kutta schemes.

2. Proposed formulations

To establish an accurate family of the time integration scheme, it is assumed that the acceleration vector is a complete *m*th order polynomial in time. Therefore, the displacement function is a polynomial of degree m+2. This polynomial has m+3 unknown coefficients, which are determined based on the following conditions:

• The initial displacement and velocity are deployed from the end of the previous time step.

• The equation of motion is exactly satisfied at both ends of the time step.

• To determine the remaining m-1 coefficients, the square of the residual vector in the motion equation is integrated. Then, this integral is minimized.

In the nonlinear dynamic problems, the equation of motion has the coming form

$$[M]\{\ddot{u}\}+[C]\{\dot{u}\}+\{N_s\}=\{P(t)\} \tag{1}$$

where [M] and [C] are the mass and damping matrices respectively. Moreover, the internal and external load vectors are denoted by $\{N_s\}$ and $\{P(t)\}$, respectively. In addition, $\{u\}$, $\{\dot{u}\}$ and $\{\ddot{u}\}$ are one-to-one the displacement, velocity and acceleration vectors. The acceleration vector for the *i*th time step, $[t_i, t_{i+1}]$, is written as follows

$$\{\ddot{u}(\tau)\}=\sum_{k=1}^{m}\{a_k\}\tau^k+\{c\} \tag{2}$$

The time step is $\Delta t = t_{i+1} - t_i$ and $\tau = t - t_i$ is the time parameter ranging from 0 to Δt. The velocity and acceleration vectors are obtained by differentiating Eq. (2) with respect to time. These vectors have the coming shapes

$$\{\dot{u}(\tau)\}=\sum_{k=1}^{m}\{a_k\}\frac{\tau^{k+1}}{k+1}+\{c\}\,\tau+\{d\} \tag{3}$$

$$\{u(\tau)\}=\sum_{k=1}^{m}\{a_k\}\frac{\tau^{k+2}}{(k+1)(k+2)}+\frac{1}{2}\{c\}\tau^2+\{d\}\tau+\{e\} \tag{4}$$

The vectors {e} and {d} are determined using the known initial vectors at the beginning of the time step; as follows

$$\{e\}=\{u_i\}=\{u(\tau)_i\}\Big|_{\tau=0} \tag{5}$$

$$\{d\}=\{\dot{u}_i\}=\{\dot{u}(\tau)_i\}\Big|_{\tau=0} \tag{6}$$

By satisfying the equation of motion at the beginning of the time step, one can calculate the vector {c}, as below

$$\{\ddot{u}_i\}=\{c\}=-[M]^{-1}[C]\{\dot{u}_i\}-[M]^{-1}\{N_{s_i}\}+[M]^{-1}\{P_i\} \tag{7}$$

To determine the remaining unknown coefficients, m equations are required. One of them is obtained by satisfying the equation of motion at the end of time step; as follows

$$[M]\{\ddot{u}_{i+1}\}+[C]\{\dot{u}_{i+1}\}+\{N_{s_{i+1}}\}=\{P(i+1)\Delta t\}=\{P_{i+1}\} \tag{8}$$

The internal force vector at the end of the time step is predicted by

$$\{N_{s_{i+1}}\}=\{N_{s_i}\}+[K]\{\Delta u_i\} \tag{9}$$

$$\{\Delta u_i\}=\sum_{k=1}^{m}\frac{1}{(k+1)(k+2)}\{a_k\}\Delta t^{k+2}+\frac{1}{2}\{c\}\Delta t^2+\{d\}\Delta t \tag{10}$$

In Eq. (9), [K] is the tangential stiffness matrix which is computed at the beginning of each time step. Substituting Eqs. (2)-(4), (9) and (10) into Eq. (8) gives the subsequent result

$$\begin{aligned}&[M]\left[\sum_{k=1}^{m}\{a_k\}\Delta t^k+\{c\}\right]+[C]\left[\sum_{K=1}^{m}\frac{\Delta t^{k+1}}{k+1}\{a_k\}+\{c\}\Delta t+\{d\}\right]\\&+\{N_{s_i}\}+[K]\left[\sum_{k=1}^{m}\{a_k\}\frac{\Delta t^{k+2}}{(k+1)(k+2)}+\frac{1}{2}\{c\}\Delta t^2+\{d\}\Delta t\right]=\{P_{i+1}\}\end{aligned} \tag{11}$$

Eq. (11) is simplified to the next form

$$\begin{aligned}&\sum_{k=1}^{m}\left[[M]\Delta t^k+[C]\frac{\Delta t^{k+1}}{k+1}+[K]\frac{\Delta t^{k+2}}{(k+1)(k+2)}\right]\{a_k\}+\ldots\\&\left[[M]+[C]\Delta t+\frac{1}{2}[K]\Delta t^2\right]\{c\}+\ldots\\&\left[[C]+[K]\Delta t\right]\{d\}+\ldots\\&\{N_{s_i}\}=\{P((i+1)\Delta t)\}\end{aligned} \tag{12}$$

The matrix shape of Eq. (12) has the following appearance

$$[A_1]\{a_1\}+[A_2]\{a_2\}+\cdots+[A_k]\{a_k\}=[B_c]\{c\}+[B_d]\{d\}+\{N_{s_i}\}+\{P_{i+1}\} \tag{13}$$

The residual of the equation of motion can be expressed as

$$\{e(\tau)\}=[M]\{\ddot{u}(\tau)\}+[C]\{\dot{u}(\tau)\}+\{N_s(\tau+i\Delta t)\}-\{P(\tau+i\Delta t)\} \tag{14}$$

The approximation of the vector $\{N_s(\tau+i\Delta t)\}$ is given by

$$\{N_s(\tau+i\Delta t)\}=\{N_s(t_i+\tau)\}=\{N_{s_i}\}+\{\Delta N_s(\tau)\} \tag{15}$$

$$\{\Delta N_s(\tau)\}=[K]\{\Delta u(\tau)\} \tag{16}$$

Obviously, for the linear analysis, it is sufficient to use $\{N_{s_{i+1}}\}=[K]\{u_{i+1}\}$ rather than Eq. (15). Substituting Eqs. (15)-(16) and (2)-(4) into Eq. (14) results in the error vector, as follows

$$\begin{aligned}&\{e(\tau)\}=[M]\left[\sum_{k=1}^{m}\{a_k\}\tau^k+\{c\}\right]+[C]\left[\sum_{k=1}^{m}\{a_k\}\frac{\tau^{k+1}}{k+1}+\{c\}\tau+\{d\}\right]\\&+\{N_{s_i}\}+[K]\left[\sum_{k=1}^{m}\{a_k\}\frac{\tau^{k+2}}{(k+1)(k+2)}+\frac{1}{2}\{c\}\tau^2+\{d\}\tau\right]-\{P(\tau+i\Delta t)\}\end{aligned} \tag{17}$$

This equality can be simplified as

$$\begin{aligned}\{e(\tau)\}=&\sum_{k=1}^{m}\left[[M]\tau^k+[C]\frac{\tau^{k+1}}{k+1}+[K]\frac{\tau^{k+2}}{(k+1)(k+2)}\right]\{a_k\}+\ldots\\&+\left[[M]+[C]\tau+\frac{1}{2}[K]\tau^2\right]\{c\}+\ldots\\&+\left[[C]+[K]\tau\right]\{d\}+\ldots\\&\{N_{s_i}\}-\{P(\tau+i\Delta t)\}\end{aligned} \tag{18}$$

To determine the remaining unknown coefficients, the integral of square error from 0 to Δt is required. This integral can be written in the below shape

$$I=\int_0^{\Delta t}\{e(\tau)\}^T.\{e(\tau)\}d\tau=\int_0^{\Delta t}\sum_{n=1}^{N}e_n^2(\tau)d\tau \tag{19}$$

Where, N is the structural number of degrees of freedom. It should be added that $e_n(\tau)$ is the nth component of vector $\{e(\tau)\}$.

To develop a scheme with high accuracy, the integral of square error is minimized over each time step. To do this, the first-order derivatives of Eq. (19) with respect to the remaining unknown coefficients are equated to zero, i.e.,

$$\left\{\frac{\partial I}{\partial\{a_l\}}\right\}=\circ\Rightarrow\left\{\frac{\partial I}{\partial\{a_l\}}\right\}=\int_0^{\Delta t}\frac{\partial}{\partial\{a_l\}}\left[\{e(\tau)\}^T.\{e(\tau)\}\right]d\tau=\{\circ\}_{n\times 1} \tag{20}$$

Using the chain rule, one can determine the derivative of square error, as follows (Graham 1982)

$$\frac{\partial(e^T.e)}{\partial\{a_i\}}=\frac{\partial\{e\}}{\partial\{a_i\}}\times(2\times\{e\}) \tag{21}$$

The matrix $\frac{\partial(\{e(\tau)\})}{\partial\{a_l\}}$ is calculated by considering Eq. (18). Using the vector differential rules, which is mentioned in (Graham 1982), one can obtain the following result

$$\begin{aligned}&\frac{\partial\{e(\tau)\}}{\partial\{a_l\}}=\frac{\partial}{\partial\{a_l\}}\left\{\sum_{k=1}^{m}\left[[M]\tau^k+[C]\frac{\tau^{k+1}}{k+1}+[K]\frac{\tau^{k+2}}{(k+1)(k+2)}\right]\{a_k\}\right\}+..\\&\frac{\partial}{\partial\{a_l\}}\left\{\left[[M]+[C]\tau+\frac{1}{2}[K]\tau^2\right]\{c\}\right\}+\ldots\\&\frac{\partial}{\partial\{a_l\}}\{[[C]+[K]\tau]\{d\}\}+\frac{\partial\{N_{si}\}}{\partial\{a_l\}}-\frac{\partial\{P(\tau+i\Delta t)\}}{\partial\{a_l\}}\end{aligned} \tag{22}$$

Utilizing relation (22) and employing the equalities $\frac{\partial\{a_k\}}{\partial\{a_l\}}_{k\neq l}=\{\circ\}$ and $\frac{\partial\{a_k\}}{\partial\{a_l\}}_{k=l}=I_{n\times n}$, the next equation is derived

$$\frac{\partial\{e(\tau)\}}{\partial\{a_l\}}=\left[[M]\tau^l+[C]\frac{\tau^{l+1}}{l+1}+[K]\frac{\tau^{l+2}}{(l+1)(l+2)}\right]^T \tag{23}$$

Consequently, Eq. (20) can be expressed as below

$$\left\{\frac{\partial I}{\partial\{a_l\}}\right\}=\int_0^{\Delta t}\frac{\partial}{\partial\{a_l\}}\left[\{e(\tau)\}^T.\{e(\tau)\}\right]d\tau=2\int_0^{\Delta t}\frac{\partial\{e(\tau)\}}{\partial\{a_l\}}\{e(\tau)\}d\tau=\{\circ\} \tag{24}$$

$$\int_{\circ}^{\Delta t}\left[[M]\tau^{l}+[C]\frac{\tau^{l+1}}{l+1}+[K]\frac{\tau^{l+2}}{(l+1)(l+2)}\right]^{T}\{e(\tau)\}d\tau=\{\circ\} \tag{25}$$

Substituting Eq. (20) into Eq. (25) gives the subsequent result

$$\begin{gathered}\left[\int_{\circ}^{\Delta t}\left[[M]\tau^{l}+[C]\frac{\tau^{l+1}}{l+1}+[K]\frac{\tau^{l+2}}{(l+1)(l+2)}\right]^{T}\left[[M]+[C]\tau+\frac{1}{2}[K]\tau^{2}\right]d\tau\right]\{c\}+\ldots\\ \sum_{k=1}^{m}\left[\int_{\circ}^{\Delta t}\left[[M]\tau^{l}+[C]\frac{\tau^{l+1}}{l+1}+[K]\frac{\tau^{l+2}}{(l+1)(l+2)}\right]^{T}\left[[M]\tau^{k}+[C]\frac{\tau^{k+1}}{k+1}+[K]\frac{\tau^{k+2}}{(k+2)(k+1)}\right]d\tau\right]\{a_{k}\}+\ldots\\ \left[\int_{\circ}^{\Delta t}\left[[M]\tau^{l}+[C]\frac{\tau^{l+1}}{l+1}+[K]\frac{\tau^{l+2}}{(l+1)(l+2)}\right]^{T}[[C]+[K]\tau]d\tau\right]\{d\}+\ldots\\ \left[\int_{\circ}^{\Delta t}\left[[M]\tau^{l}+[C]\frac{\tau^{l+1}}{l+1}+[K]\frac{\tau^{l+2}}{(l+1)(l+2)}\right]^{T}\{N_{s_i}\}d\tau\right]=\\ \left[+\int_{\circ}^{\Delta t}\left[[M]\tau^{l}+[C]\frac{\tau^{l+1}}{l+1}+[K]\frac{\tau^{l+2}}{(l+1)(l+2)}\right]^{T}\{P(\tau+i\Delta t)\}d\tau\right]\end{gathered} \tag{26}$$

This equality can be written in the matrix form as

$$\sum_{k=1}^{m}[V_{lk}]\{a_{k}\}=[V_{lc}]\{c\}+[V_{ld}]\{d\}+[V_{\ln}]\{N_{s_i}\}+\{V_{lp}\} \tag{27}$$

As a result, the following m+1 equations are now available to find the unknown coefficients

$$\begin{gathered}l=1\quad [V_{11}]\{a_1\}+[V_{12}]\{a_2\}+\cdots[V_{1m}]\{a_m\}=[V_{1c}]\{c\}+[V_{1d}]\{d\}+[V_{1n}]\{N_{s_i}\}+\{V_{1p}\}\\ l=2\quad [V_{21}]\{a_1\}+[V_{22}]\{a_2\}+\cdots[V_{2m}]\{a_m\}=[V_{2c}]\{c\}+[V_{2d}]\{d\}+[V_{2n}]\{N_{s_i}\}+\{V_{2p}\}\\ \vdots\\ l=m:[V_{m1}]\{a_1\}+[V_{m2}]\{a_2\}+\cdots+V_{m,m}\{a_m\}=[V_{mc}]\{c\}+[V_{md}]\{d\}+[V_{kn}]\{N_{s_i}\}+\{V_{kp}\}\\ [A_1]\{a_1\}+[A_2]\{a_2\}+\cdots+[A_m]\{a_m\}=[B_c]\{c\}+[B_d]\{d\}+[I]\{N_{s_i}\}+\{p\}\end{gathered} \tag{28}$$

Since the number of equations is greater than the number of unknowns, one equation should be removed. Based on the computer evaluation, it can be shown that eliminating the last part of Eq. (28) yields more accurate results. By solving the remaining equations of (28), the unknown coefficients are determined. Finally, the solution vectors at the end of the *i*th time step can be determined, as follows

$$\begin{cases}\{u_{i+1}\}=\sum_{k=1}^{m}\frac{\Delta t^{k+2}}{(k+1)(k+2)}\{a_k\}+\frac{1}{2}\Delta t^{2}\{c\}+\Delta t\{d\}+\{e\}\\ \{\dot{u}_{i+1}\}=\sum_{k=1}^{m}\frac{\Delta t^{k+1}}{k+1}\{a_k\}+\Delta t\{c\}+\{d\}\\ \{\ddot{u}_{i+1}\}=\sum_{k=1}^{m}\Delta t^{k}\{a_k\}+\{c\}\end{cases} \tag{29}$$

3. Amplification matrix

To assess the accuracy and stability of the new time integration technique, it is necessary to derive the amplification matrix. To reach this goal, the subsequent single degree-of-freedom system is considered

$$\ddot{x}+2\xi\omega\dot{x}+\omega^{2}x=0 \tag{30}$$

where x is a scalar variable, ω is the circular frequency of free vibration and ξ is the damping ratio. If the suggested method is used to find the solution for the mentioned linear

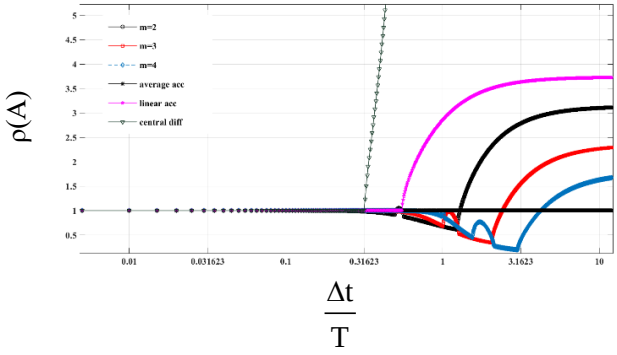

Fig. 1 Spectral radii versus Δt/T for several methods (ξ=0)

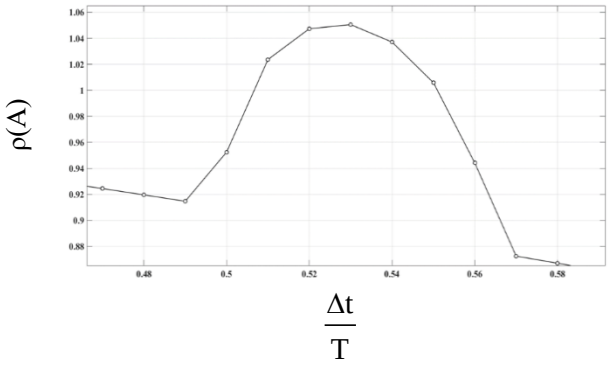

Fig. 2 Spectral radius of the proposed method for m=2 and ksi=0

system, the following recursive relationship is obtained

$$\left\{x_{n+1}\quad \dot{x}_{n+1}\right\}^{T}=[A]\left\{x_{n}\quad \dot{x}_{n}\right\}^{T} \tag{31}$$

where [A] is the amplification matrix of the new tactic. All the entries of this matrix are provided in Appendix A.

4. Stability

The stability of a time integration method depends on the spectral radius of the amplification matrix. The spectral radius of [A], $\rho(A)$, is defined in the below form

$$\rho(A)=\max\left|\lambda_{i}\right| \tag{32}$$

where λ_i is the *i*th eigenvalue of [A]. If the condition $\rho(A)\leq 1$ is satisfied, then the proposed technique is stable (Bathe 2006). In Figs. 1-4, the spectral radii are plotted versus Δt/T for different values of damping ratio.

From Fig. 1, it can be concluded that the stability domain increases when the order of approximating polynomial, m, increases. For m=2, the present method is stable when $\Delta t/T\leq 1.29$. As it is demonstrated in Fig. 1, the critical time step for m=3 and m=4 are 2.409 and 4.238, respectively. It should be reminded that the critical time step for the central difference and linear acceleration methods are $1/\pi\approx 0.33$ and $\sqrt{3}/\pi\approx 0.55$ correspondingly. Based on these values, the stability limit for authors' technique is

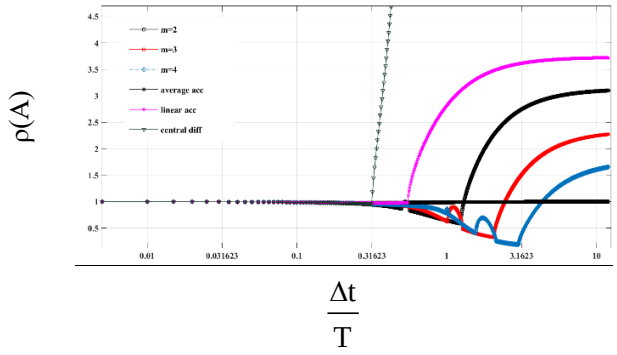

Fig. 3 Spectral radius versus $\Delta t/T$ for several methods (ξ=0.02)

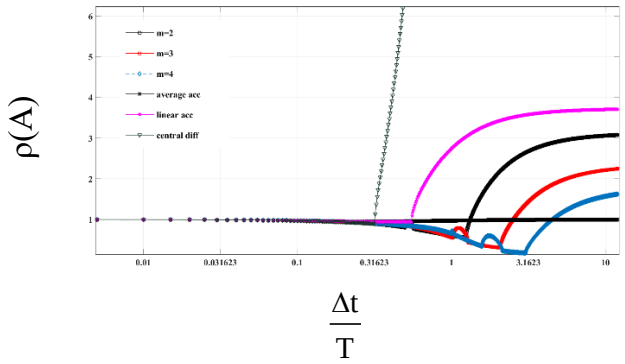

Fig. 4 Spectral radius versus Δt/T for several methods (ξ=0.05)

Table 1 Stability limit of the scheme for different values of damping ratio

	$\xi=0$	$\xi=0.02$	$\xi=0.05$	$\xi=0.1$
m=2	1.2904	1. 3040	1.3238	1.3579
m=3	2.4090	2.4529	2.5202	2.6360
m=4	4.2382	4.3511	4.5260	4.8318

considerably greater than that of the central difference and linear acceleration tactics.

According to Fig. 2, the suggested approach for m=2 and ξ=0 suffers from a local instability which occurs in the range of Δt/T between 0.505 and 0.55. A similar phenomenon is observed in the previous developed schemes (Golley 1996, Razavi *et al.* 2007). It is interesting to note that this local instability does not exist for m=3 and m=4. In addition, the local instability for m=2 does not occur when the damping ratio is greater than 2%, as shown in Figs. 3-4. Table 1, shows the stability limit of the present technique for different values of damping ratio. Based on this table, it can be concluded that the domain of stability for the new technique increases when the damping ratio is greater than zero.

5. Numerical accuracy

The accuracy of a numerical integration method is investigated by the order of accuracy, numerical dissipation and numerical dispersion of the scheme. Later in section 6, the order of accuracy for the presented approach is discussed. Numerical dissipation and numerical dispersion of the method are measured using the eigenvalues of the amplification matrix, as follows (Hilber *et al.* 1977)

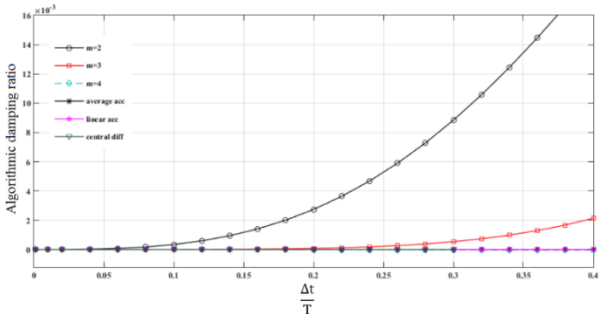

Fig. 5 Algorithmic damping ratio of the proposed method, compared with the other schemes

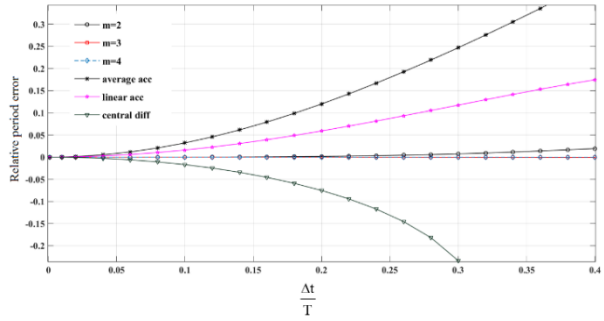

Fig. 6 Relative period error of the proposed method, compared with the other schemes

$$\lambda_{1,2} = A \pm iB = e^{(-\overline{\xi}\overline{\omega} \pm i\overline{\omega}_d)\Delta t} \tag{33}$$

$$\overline{\omega} = \frac{\arctan(B/A)}{\sqrt{1-\xi^2}\Delta t} \tag{34}$$

$$\overline{\omega}_d = \overline{\omega}\sqrt{1-\xi^2} \tag{35}$$

$$\overline{\xi} = -\frac{\ln(A^2+B^2)\sqrt{1-\xi^2}}{2\arctan(B/A)} \tag{36}$$

Where, λ_1 and λ_2 are the eigenvalues of the amplification matrix. Numerical dissipation is measured by the algorithmic damping ratio $\overline{\xi}$. In addition, the measure of numerical dispersion is provided by the relative period error $(\overline{T}-T)/T$, where $T=2\pi/\omega$ is the period of vibration and $\overline{T}=2\pi/\overline{\omega}$ is the algorithmic counterpart of T. In Figs. 5-6, algorithmic damping ratio and relative period error of authors' scheme are compared with the other well-known techniques.

Fig. 5, demonstrates the proposed method has numerical

Table 2 Numerical results and corresponding errors of Eq. (43)

Time (sec)	Proposed (m=2)		Proposed (m=3)		Proposed (m=4)		Average Acc.		Linear Acc.		Central Diff.		Runge-Kutta 2		Runge-Kutta 4	
	u	|err|	u	|err|	u	|err|	u	|err|	u	|err|	u	|err|	u	|err|	u	|err|
0	1	0	1	0	1	0	1	0	1	0	1	0	1	0	1	0
1	0.5403	4.80E-07	0.5403	4.51E-09	0.5403	5.70E-12	0.5410	0.0007	0.5407	0.0004	0.5400	0.0004	0.5390	0.0013	0.5403	6.61E-07
2	-0.4161	2.55E-06	-0.4161	9.03E-09	-0.4161	3.03E-11	-0.4146	0.0015	-0.4154	0.0008	-0.4169	0.0008	-0.4193	0.0031	-0.4161	1.57E-06
3	-0.9900	4.35E-06	-0.9900	1.40E-09	-0.9900	5.17E-11	-0.9896	0.0004	-0.9898	0.0002	-0.9902	0.0002	-0.9911	0.0011	-0.9900	5.58E-07
4	-0.6536	2.37E-06	-0.6536	1.58E-08	-0.6536	2.81E-11	-0.6562	0.0025	-0.6549	0.0013	-0.6524	0.0013	-0.6489	0.0047	-0.6536	2.33E-06
5	0.2837	3.64E-06	0.2837	2.36E-08	0.2837	4.32E-11	0.2797	0.0040	0.2817	0.0020	0.2857	0.0020	0.2918	0.0081	0.2837	4.08E-06
6	0.9602	8.51E-06	0.9602	6.94E-09	0.9602	1.01E-10	0.9588	0.0014	0.9595	0.0007	0.9609	0.0007	0.9636	0.0035	0.9602	1.79E-06
7	0.7539	6.10E-06	0.7539	2.43E-08	0.7539	7.24E-11	0.7577	0.0038	0.7558	0.0019	0.7520	0.0019	0.7469	0.0070	0.7539	3.45E-06
8	-0.1455	3.54E-06	-0.1455	3.92E-08	-0.1455	4.21E-11	-0.1389	0.0066	-0.1422	0.0033	-0.1488	0.0033	-0.1588	0.0133	-0.1455	6.65E-06
9	-0.9111	1.22E-05	-0.9111	1.64E-08	-0.9111	1.45E-10	-0.9080	0.0031	-0.9096	0.0016	-0.9127	0.0015	-0.9182	0.0071	-0.9111	3.65E-06
10	-0.8391	1.05E-05	-0.8391	2.92E-08	-0.8391	1.25E-10	-0.8436	0.0045	-0.8413	0.0023	-0.8368	0.0023	-0.8310	0.0081	-0.8391	3.94E-06

Table 3 Maximum absolute errors of u, $\dot{u}$ and $\ddot{u}$

Max Absolute Error of	m=2	m=3	m=4	Average Acc	Linear Acc	Central Diff	Runge-Kutta 2	Runge-Kutta 4
u	1.3103E-5	3.9241E-8	1.5577E-10	6.5890E-3	3.2950E-3	3.3008E-3	1.3297E-2	6.6602E-6
$\dot{u}$	1.0867E-5	4.7265E-8	1.2919E-10	7.8847E-3	4.0067E-3	9.9833E-2	1.5913E-2	7.9655E-6
$\ddot{u}$	1.3103E-5	3.9241E-8	1.5577E-10	6.5890E-3	3.2950E-3	9.9313E-2	1.3297E-2	6602E-6

dissipation which is an essential property to damp out the spurious high-frequency responses (Fung 2003). In the contrary, the average acceleration, linear acceleration and central difference methods have no numerical dissipation. As it is shown in Fig. 5, by increasing the order of approximating polynomial, the amount of the numerical dissipation is decreased.

Fig. 6, clearly demonstrates that the suggested technique has considerably smaller period error than the other schemes. Moreover, this figure shows that by increasing the order of the method, the period error rapidly decreases. For instance, period error of the central difference, average acceleration and linear acceleration methods at $\Delta t/T=0.2$ are -0.075, 0.12 and 0.059, respectively. This error for the proposed method is 0.001 when m=2, and it is zero when m=3 and m=4.

6. Order of accuracy

To assess the order of accuracy of the scheme, the numerical amplification matrix should be compared with the analytical one. The coefficients of the amplification matrix for m=2 to 4 are provided in Appendix A. In order to derive the analytical amplification matrix, the equation of motion for the SDOF model with zero external loading is considered, as follows

$$\ddot{x}+2\xi\omega\dot{x}+\omega^2 x=0 \tag{37}$$

This equation can be changed into the subsequent equivalent first-order differential equation

$$\dot{Y}=AY \tag{38}$$

where

$$Y=\begin{Bmatrix} x \\ \dot{x} \end{Bmatrix} \text{ and } A=\begin{bmatrix} 0 & 1 \\ -\omega^2 & -2\xi\omega \end{bmatrix} \tag{39}$$

The exact solution for Eq. (38) with given initial vector Y_0 can be expressed as (Levine 1996, Turyn 2013)

$$Y=e^{At}Y_0 \tag{40}$$

Therefore, the following recursive relationship is obtained

$$Y_{i+1}=e^{A\Delta t}Y_i \tag{41}$$

The matrix $e^{A\Delta t}$ can be calculated using the Taylor series expansion, as below

$$e^{At}=I+tA+\frac{t^2}{2!}A^2+\frac{t^3}{3!}A^3+\ldots \rightarrow e^{A\Delta t}=I+\Delta tA+\frac{\Delta t^2}{2!}A^2+\frac{\Delta t^3}{3!}A^3+\ldots \tag{42}$$

By employing Eq. (42), the coefficients of the analytical amplification matrix are determined and given in Appendix A. Comparing the coefficients of the amplification matrix for the proposed method with the analytical ones proves that the suggested approach has the third-order accuracy for m=2. It is interesting to note that the fourth and fifth orders of accuracy are provided for m=3 and m=4, respectively. Generally, the proposed method has m+1 order of accuracy. It should be reminded that the central difference, average acceleration and linear acceleration methods have only

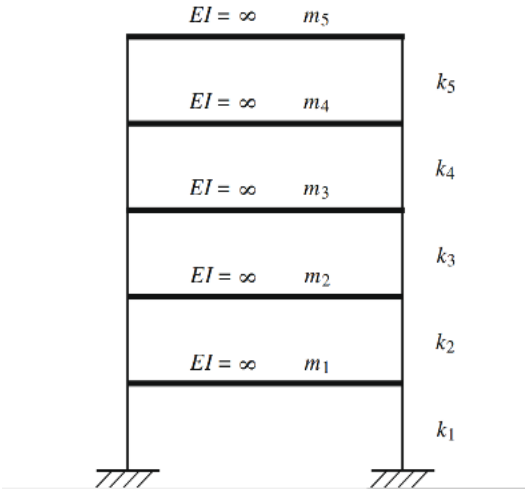

Fig. 7 Five story shear frame

second-order accuracy.

7. Numerical examples

In this section, the accuracy and stability of the suggested technique are investigated using several numerical examples. These problems are a single-degree-of-freedom oscillator, a five-story shear frame structure with classical and non-classical damping, a two-DOF structure subjected to impact loads, a linear and non-linear plane truss, a two-DOF system with non-linear behavior and three-dimensional nonlinear trusses.

7.1 Undamped single degree of freedom

As a first example, the following second-order ordinary differential equation is considered. This equation has been extensively used to assess the accuracy characteristics of the several time integration algorithms (Bathe 2006).

$$\ddot{u}+u=0 \tag{43}$$

With the initial conditions u_0=1 and $\dot{u}_0=0$, the exact solution of Eq. (43) is u_{exact}=cos(t) (Rezaiee-Pajand and Karimi-Rad 2015). This problem is solved using the members of the Newmark scheme, the second-order Runge-Kutta method (RK2), the fourth order Runge-Kutta algorithm (RK4) and authors' technique. The time step is selected to be Δt=0.1 s. The error is defined as the difference between the exact response and that obtained by the numerical integration methods. Table 2, demonstrates the numerical results for u along with the corresponding errors. Table 3 shows the maximum absolute errors of u, $\dot{u}$ and $\ddot{u}$.

Based on Tables 2-3, it can be concluded that the presented algorithm gives considerably more precise results than the other methods. The results of the RK4 approach are better in some points than those of the proposed method with m=2. However, for m=3 and m=4, the error of the suggested scheme is always smaller than that of the other methods.

Table 4 The displacements and velocities at the top story of the five-story frame

Scheme	Res.	Time(sec) 0.2	0.4	0.6	0.8	1	Max error(%)
Exact	u_5	0.0040357	0.0263841	0.0532948	0.0548026	0.0198097	
	$\dot{u}_5$	0.0590925	0.1490397	0.0933473	-0.0899645	-0.2385299	
m=2	u_5	0.0040357	0.0263841	0.0532948	0.0548026	0.0198097	0.000
	$\dot{u}_5$	0.0590926	0.1490397	0.0933473	-0.0899643	-0.2385299	0.000
m=3	u_5	0.0040357	0.0263841	0.0532948	0.0548026	0.0198097	0.000
	$\dot{u}_5$	0.0590924	0.1490397	0.0933473	-0.0899645	-0.2385299	0.000
m=4	u_5	0.0040357	0.0263841	0.0532948	0.0548026	0.0198097	0.000
	$\dot{u}_5$	0.0590924	0.1490397	0.0933473	-0.0899645	-0.2385299	0.000
Average Acc	u_5	0.0040387	0.0263717	0.0532790	0.0548077	0.0198357	0.131
	$\dot{u}_5$	0.0590506	0.1490644	0.0934016	-0.0897864	-0.2385089	0.198
Linear Acc	u_5	0.0040347	0.0263760	0.0532878	0.0548081	0.0198241	0.073
	$\dot{u}_5$	0.0590671	0.1490482	0.0933736	-0.0898688	-0.2385148	0.106
Central Diff	u_5	0.0040265	0.0263846	0.0533052	0.0548088	0.0198008	0.229
	$\dot{u}_5$	0.0536919	0.1475472	0.0998641	-0.0799380	-0.2345211	11.145
Runge Kutta 2	u_5	0.0040282	0.0264025	0.0533141	0.0547809	0.0197529	0.287
	$\dot{u}_5$	0.0591525	0.1489601	0.0932215	-0.0903063	-0.2385251	0.380
Runge kutta 4	u_5	0.0040357	0.0263841	0.0532948	0.0548026	0.0198097	0.000
	$\dot{u}_5$	0.0590925	0.1490400	0.0933475	-0.0899642	-0.2385299	0.000

7.2 A five-story shear frame

Fig. 7, shows a five-story shear building which is analyzed by Wang and Au (2009). The lumped masses for all floors are the same and equal to 2.616×10^6(kg). The stiffness coefficients are assumed to be $k_1=1177.2\times10^6$(N/m) and $k_2=k_3=k_4=k_5=981\times10^6$(N/m). The classical damping matrix is determined using $[C]=0.3[M]+0.002[K]$. To consider the effect of the damper device installed at the first floor, the term $20C_{11}$ is also added to the first degree of freedom. This building is subjected to the subsequent lateral loads:

The displacement and velocity at the top story of the shear building are computed using several time integration schemes with Δt=0.01 s. Table 4, shows the numerical results. For comparison purposes, the exact results along with the maximum errors are also listed in this table. The error is defined as the difference between the exact response and that obtained by the numerical algorithms.

$$P=2.616\times10^6\{1\ 1\ 1\ 1\ 1\}^T\sin(\pi t) \tag{44}$$

According to Table 4, it can be concluded that the errors of the RK4 and proposed methods are zero to four decimal places. Indeed, these schemes give considerably more precise responses in comparison with the RK2 and Newmark algorithms. It is interesting to note that the errors of authors' technique are zero to seven decimal places except for the velocity at the end of the first time step. As a result, the suggested approach is more accurate than the

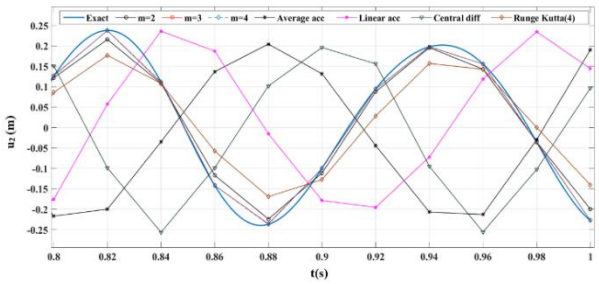

Fig. 8 Time histories of displacement u_2

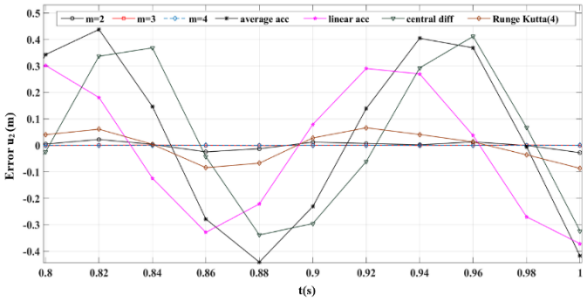

Fig. 9 The curves of errors in u_2

RK4 technique.

7.3 A two DOF model

Some researchers analyzed a two DOF structure subjected to a triangular impulse (Shishvan *et al.* 2009, Rezaiee-Pajand and Sarafrazi 2010). The equation of motion for this system and the function of applied force are given below

$$\begin{bmatrix} m & 0 \\ 0 & 3m \end{bmatrix} \ddot{u} + \begin{bmatrix} 3k & -2k \\ -2k & 6k \end{bmatrix} u = \begin{Bmatrix} 0 \\ P(t) \end{Bmatrix} \tag{45}$$

$$P(t) = \begin{cases} 1000(1-10t) & 0 \le t \le 0.1 \\ 0 & t \ge 0.1 \end{cases} \tag{46}$$

The values of k and m are 1000 (N/m) and 0.5 (kg), respectively. The natural frequencies and the mode matrix of this two DOF system are computed as

$$\begin{cases} \omega_1 = 49.8336 \text{ rad/s} \\ \omega_2 = 86.6984 \text{ rad/s} \end{cases} \tag{47}$$

$$\Phi = \begin{bmatrix} 0.7763 & 1.1821 \\ 0.6825 & -04482 \end{bmatrix} \tag{48}$$

This problem is solved using several time integration methods with Δt=0.02 s. Fig. 8, demonstrates the numerical results along with the exact solution. In addition, the numerical errors which are defined as the absolute difference between the exact and numerical response are depicted in Fig. 9. The solution obtained by deploying the presented technique is considerably closer to the exact solution in comparison with the other approaches, as demonstrated in Fig. 8. Moreover, as the order of the method (m) increases, the error of the suggested algorithm decreases. It should be added that the solution of the RK2 approach becomes infinity. Based on the obtained responses, the new scheme gives better results than the RK4 algorithm. Fig. 9, shows that the error for m=3 is almost the same as m=4.

Table 5 Structural properties of plane truss

Member	Area(mm^2)	Length(mm)	$E\left(\frac{N}{m^2}\right)$	$\bar{m}\left(\frac{N.\,Sec^2}{m^2}\right)$
1	6451.6	1524	2.06844×10^{11}	689.48
2	6451.6	2155.3	2.06844×10^{11}	689.48
3	6451.6	1524	2.06844×10^{11}	689.48

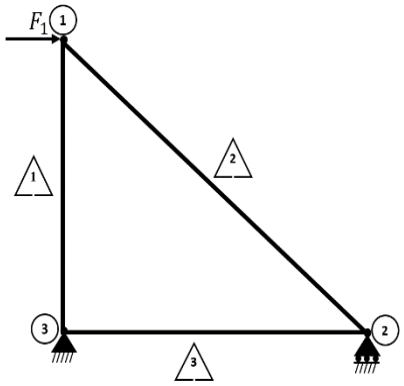

Fig. 10 Plane truss

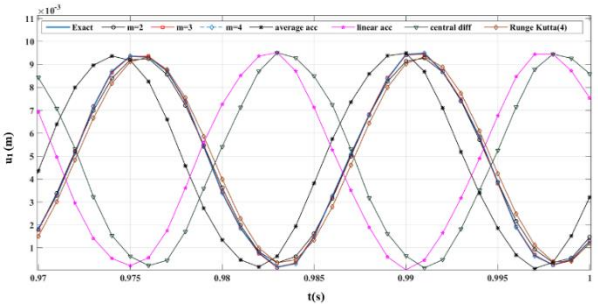

Fig. 11 The horizontal displacement at joint 1 for plane truss

7.4 Linear analysis of a plane truss

Fig. 10, shows a plane truss with three degrees of freedom, which is analyzed using several time integration methods (Paz and Leigh 1985). Table 5, demonstrates the geometry and material properties of this problem. The horizontal displacement at joint 1 to the force F_1=22241.108 N is determined with Δt=0.001. The numerical results along with the exact solution are demonstrated in Fig. 11.

The numerical errors are depicted in Fig. 12. This figure clearly shows that the best results obtained by using the proposed scheme. The second most accurate results are

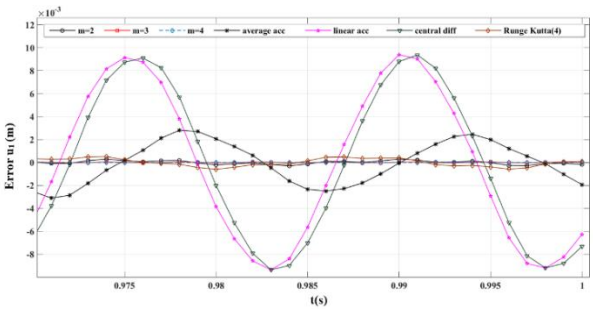

Fig. 12 The curves of errors in horizontal displacement at joint 1 for plane truss

Table 6 Modified cross-sectional areas for plane truss

Member	Area(mm^2)
1	64.516
2	64.516
3	64.516

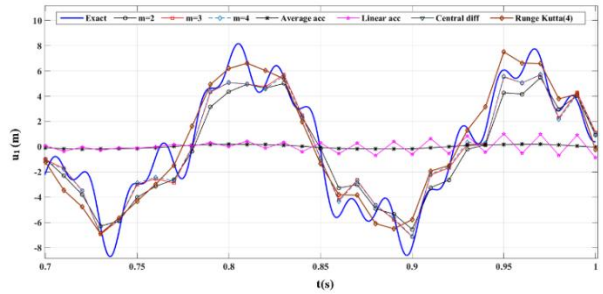

Fig. 13 The horizontal displacement at joint 1 for plane truss

provided by the RK4 technique. As shown in Fig. 12, the linear acceleration and central difference methods give the worst answers.

7.5 Nonlinear analysis of a plane truss

According to the Table 6, the cross-sectional areas of the plane truss shown in Fig. 10 are considerably reduced. As a result, large displacements occur in this structure, so geometrically nonlinear behavior should be considered. The horizontal displacement at joint 1, which is subjected to a harmonic force $F_1 = 2224.110\times10^3 \sin(310t)$ N , is computed using several time integration algorithms with Δt=0.01 s. The numerical results are depicted in Fig. 13. For comparison purposes, the approximate exact solution, which is determined using the RK4 technique with a very fine time step of Δt=0.0001 s, is added to Fig. 13. To demonstrate the performances of the mentioned methods, the numerical errors are shown in Fig. 14.

According to Figs. 13-14, the most precise solutions are obtained by authors' technique and the RK4 methods. The linear and average acceleration schemes give the worst results. It is interesting to note that the response computed with m=3 is in good agreement with the solution determined with m=4. In this example, the proposed process with m=3 provides accurate results with less

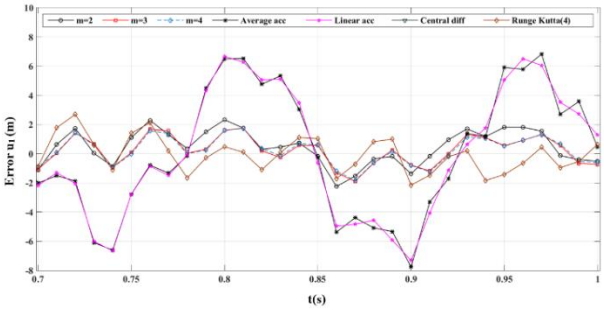

Fig. 14 The curves of errors in horizontal displacement at joint 1 for plane truss

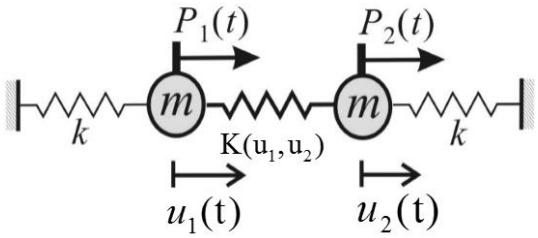

Fig. 15 A 2-DOF spring-mass system

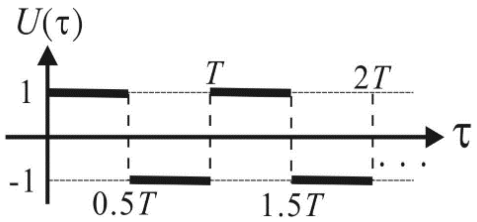

Fig. 16 The load function for the 2-DOF spring-mass system

computational effort than the scheme with m=4.

7.6 A 2-DOF model with nonlinear spring

Fig. 15, shows a 2-DOF spring-mass system which has two edge linear springs with constant k and a middle nonlinear spring (Kuo *et al.* 2012). The equation of motion for this system can be described as below

$$\begin{cases} \ddot{u}_1 + u_1 + \left[1-(u_2-u_1)^2\right]\times(u_1-u_2) = -1.5U(\tau) \\ \ddot{u}_2 + u_2 + \left[1-(u_2-u_1)^2\right]\times(u_2-u_1) = 0.5U(\tau) \end{cases} \quad (49)$$

where U(τ) is the load function, and it is given in Fig. 16.

Following reference (Kuo *et al.* 2012), the initial conditions are assumed to be $u_1 = u_2 = 0$, $\dot{u}_1 = 1.32994$ and $\dot{u}_2 = -0.91696$. Selecting Δt=T/40 and T=1.53229, this problem is solved using several time integration schemes. Fig. 17, demonstrates the time histories of the response u_1. Moreover, the absolute differences between the exact and numerical solution are depicted in Fig. 18.

From Fig. 18, it can be concluded that the numerical error for all members of the suggested approach is almost

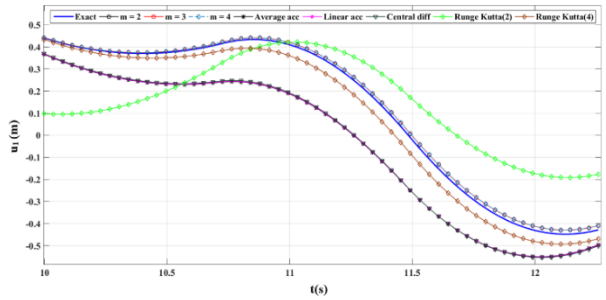

Fig. 17 Time histories of displacement u_1

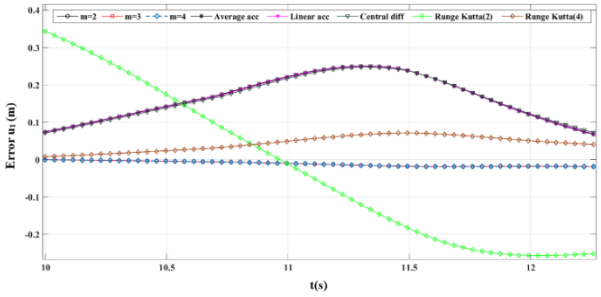

Fig. 18 The curves of errors in u_1

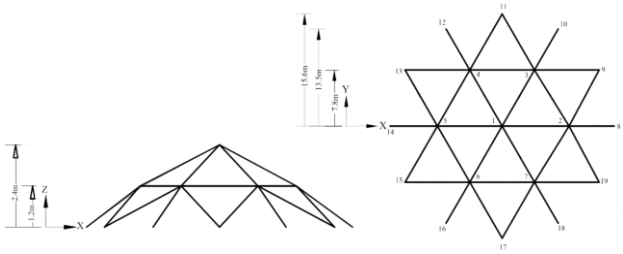

Fig. 19 3D pin-jointed truss dome

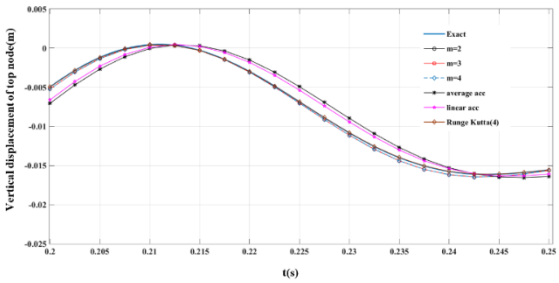

Fig. 20 Time histories of the vertical displacement for 3D truss dome

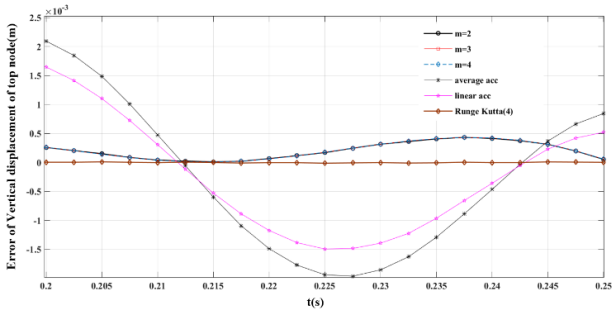

Fig. 21 The curves of errors in vertical displacement for 3D truss dome

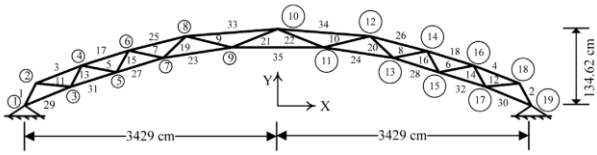

Fig. 22 A 2D arch truss

zero. After that, the RK4 scheme is in the second rank. The worst results are obtained by the RK2 technique.

7.7 A 3D pin-jointed truss dome

In this section, a three-dimensional pin-jointed dome shown in Fig. 19 is analyzed by using several time integration methods (Saka 1990). The material mass density, modulus of elasticity and cross-sectional area of all members are 7860 kg/m^3, 2.1×10^{11} N/m^2 and 3000 mm^2 respectively. The initial displacement and velocity are assumed to be zero. Joints 1, 2, ..., 7 are subjected to the vertical constant loads that its magnitude is 60000 N.

Fig. 20, shows the vertical displacement of the top truss joint versus the time. The numerical results are computed with Δt=0.0025 s. In addition, the near exact solution is determined by utilizing the RK4 scheme with a very fine time step of Δt=0.000025 s. The numerical errors for several algorithms are plotted in Fig. 21. Base on this figure, the best result is obtained using the RK4 technique. The suggested approach with m=4 is in the second rank. Both choices of m=2 and m=3 give acceptable and accurate solutions. It should be added that in this problem, the RK2 method becomes unstable and the average acceleration and linear acceleration algorithms produce inaccurate responses.

7.8 An arch truss

Fig. 22, demonstrates a 2D truss that has 19 joints and 35 members. Node numbers are shown by the circle in this figure. Tables 7-8 give the nodal coordinates and the cross-section areas of the members, respectively. The initial displacement and velocity are assumed to be zero. The elasticity modulus and the material mass density are E=6496400 N/cm^2 and ρ=7860×10^{-6} kg/cm^3, respectively (Torkamani and Shieh 2011, Rezaiee-Pajand and Estiri 2016). The load $P(t) = -15 \times 10^6[sin(\pi t) + 10\sin(200\pi t)]$ N is applied to horizontal direction of joint 10.

Using Δt=0.0075 s, the horizontal displacement at the joint 10 is computed by several time integration schemes, and it is plotted in Fig. 23. The numerical errors for various algorithms are depicted in Fig. 24. It should be added that the near exact solution is determined by the RK4 technique with a fine time step of Δt=0.00001 s. According to Fig. 24, the most precise results are obtained by the new method with m=4, m=3 and m=2 respectively. The RK4 approach is in the fourth rank and the worst results are obtained by the RK2 method. Among the members of Newmark method, the linear acceleration tactic gives the more accurate response.

Table 7 Nodal coordinates of the arch truss

Node	1 & 19	2 & 18	3 & 17	4 &16	5 & 15	6 & 14	7 & 13	8 & 12	9 & 11	10
X(cm)	3429	3048	2667	2286	1905	1524	1143	762	381	0
Y(cm)	0	50.65	34.75	83.82	65.3	110.85	87.99	128.5	100.65	134.6

Table 8 The cross-section area of the members of the arch truss

Member	1-10 & 35	11 & 12	13-16	17 & 18	19-22	23 & 24	25 & 26	27 & 28	29-32	33 & 34
Cross-section areas(cm^2)	51.61	64.52	83.87	96.77	103.23	161.29	193.55	258.06	290.32	309.68

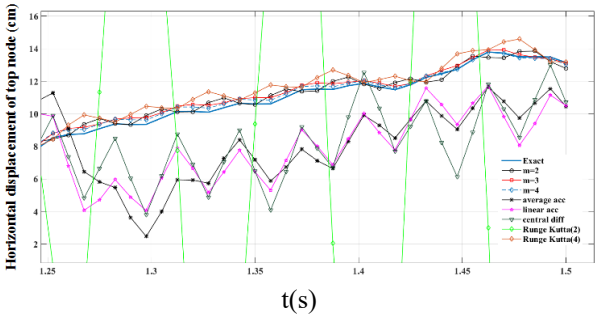

Fig. 23 Time histories of the horizontal displacement at joint 10 for 2D arch truss

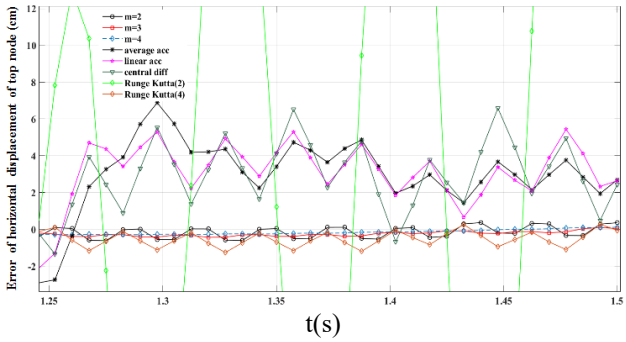

Fig. 24 The curves of errors in horizontal displacement at joint 10 for 2D arch truss

8. Conclusions

In this article, a new time integration method was proposed, in which the acceleration vector in each time step was assumed to be a complete *m*th order polynomial in time. The proposed formulation can be applied to both linear and non-linear dynamic analysis. One of the suggested technique's merits is its high accuracy, which can be enhanced by increasing the order of the method. Indeed, the order of accuracy for the new algorithm is m+1. The proposed scheme has an acceptable region of stability, which is greater than that of the central difference and linear acceleration techniques. It is interesting to note that the domain of stability becomes larger by increasing the order of the new method. However, for m=2, the suggested approach suffers from a local instability, which does not exist when the damping ratio is greater than 2%. Furthermore, this local instability does not occur for m>2.

The numerical dispersion error of the present approach is almost zero, and it is considerably smaller than that of the linear acceleration, average acceleration and central difference techniques. In fact, the proposed method has numerical dissipation, which decreases by increasing the order of approximating polynomial. The suggested tactic is self-starting, and no special starting procedure is required. Several problems were solved using the new developed algorithm to test the capability of the proposed scheme, including a five-story shear frame structure with classical and non-classical damping, a 2-DOF structure subjected to impact loads, a linear and a nonlinear plane truss, a 2-DOF system with nonlinear behavior and three-dimensional nonlinear trusses. The findings highlighted the noble performance of the suggested technique. Moreover, a comparison of the results indicated that the new scheme is considerably more accurate than the RK4, linear acceleration, average acceleration and central difference methods.

References

Alamatian, J. (2013), "New implicit higher order time integration for dynamic analysis", *Struct. Eng. Mech.*, **48**(5), 711-736.

Bathe, K.J. (2006), *Finite Element Procedures*, Klaus-Jurgen Bathe.

Bathe, K.J. (2007), "Conserving energy and momentum in nonlinear dynamics: A simple implicit time integration scheme", *Comput. Struct.*, **85**(7), 437-445.

Bathe, K.J. and Baig, M.M.I. (2005), "On a composite implicit time integration procedure for nonlinear dynamics", *Comput. Struct.*, **83**(31), A2513-2524.

Bursi, O.S., Gonzalez-Buelga, A., Vulcan, L., Neild, S.A. and Wagg, D.J. (2008), "Novel coupling Rosenbrock-based algorithms for real-time dynamic substructure testing", *Earthq. Eng. Struct. Dyn.*, **37**(3), 339-360.

Chang, S.Y. (2004), "Unconditional stability for explicit pseudodynamic testing", *Struct. Eng. Mech.*, **18**(4), 411-428.

Chang, S.Y. (2007), "Improved explicit method for structural dynamics", *J. Eng. Mech.*, **133**(7), 748-760.

Chang, S.Y. (2009), "An explicit method with improved stability property", *Int. J. Numer. Meth. Eng.*, **77**(8), 1100-1120.

Chang, S.Y. (2010), "A new family of explicit methods for linear structural dynamics", *Comput. Struct.*, **88**(11), 755-772.

Chang, S.Y. (2014), "A family of noniterative integration methods with desired numerical dissipation", *Int. J. Numer. Meth. Eng.*, **100**(1), 62-86.

Chang, S.Y. (2014), "Numerical dissipation for explicit, unconditionally stable time integration methods", *Earthq. Struct.*, **7**(2), 159-178.

Chang, S.Y. (2015), "Comparisons of structure-dependent explicit methods for time integration", *Int. J. Struct. Stab. Dyn.*, **15**(3), 1450055.

Chang, S.Y. (2016), "A virtual parameter to improve stability properties for an integration method", *Eartq. Struct.*, **11**(2), 297-313.

Chang, S.Y. (2018), "Performances of non-dissipative structure-dependent integration methods", *Struct. Eng. Mech.*, **65**(1), 91-98.

Chang, S.Y. and Liao, W.I. (2005), "An unconditionally stable explicit method for structural dynamics", *J. Earthq. Eng.*, **9**(3), 349-370.

Chang, S.Y., Wu, T.H. and Tran, N.C. (2015), "A family of dissipative structure-dependent integration methods", *Struct. Eng. Mech.*, **55**(4), 815-837.

Chang, S.Y., Wu, T.H., Tran, N.C. and Yang, Y.S. (2017),

"Applications of a family of unconditionally stable, dissipative, explicit methods to pseudodynamic tests", *Exper. Techniq.*, **41**(1), 19-36.

Chen, C. and Ricles, J.M. (2008), "Development of direct integration algorithms for structural dynamics using discrete control theory", *J. Eng. Mech.*, **134**(8), 676-683.

Chen, C., Ricles, J.M., Marullo, T.M. and Mercan, O. (2009), "Real-time hybrid testing using the unconditionally stable explicit CR integration algorithm", *Earthq. Eng. Struct. Dyn.*, **38**(1), 23-44.

Chopra, A.K. (2001), *Dynamics of Structures: Theory and Applications to Earthquake Engineering*, Prentice-Hall.

Chung, J. and Lee, J.M. (1994), "A new family of explicit time integration methods for linear and non-linear structural dynamics", *Int. J. Numer. Meth. Eng.*, **37**(23), 3961-3976.

Dokainish, M.A. and Subbaraj, K. (1989), "A survey of direct time-integration methods in computational structural dynamics-I. Explicit methods", *Comput. Struct.*, **32**(6), 1371-1386.

Felippa, C.A. and Park, K.C. (1979), "Direct time integration methods in nonlinear structural dynamics", *Comput. Meth. Appl. Mech. Eng.*, **17**, 277-313.

Fung, T.C. (1999), "Weighting parameters for unconditionally stable higher-order accurate time step integration algorithms. Part 2-second-order equations", *Int. J. Numer. Meth. Eng.*, **45**(8), 971-1006.

Fung, T.C. (2003), "Numerical dissipation in time-step integration algorithms for structural dynamic analysis", *Progr. Struct. Eng. Mater.*, **5**(3), 167-180.

Ghassemieh, M., Gholampour, A.A. and Massah, S.R. (2016), "Application of weight functions in nonlinear analysis of structural dynamics problems", *Int. J. Comput. Meth.*, **13**(1), 1650005.

Golley, B.W. (1996), "A time-stepping procedure for structural dynamics using gauss point collocation", *Int. J. Numer. Meth. Eng.*, **39**(23), 3985-3998.

Graham, A. (1982), *Kronecker Products and Matrix Calculus: With Applications*, John Wiley and Sons, Inc.

Hahn, G.D. (1991), "A modified Euler method for dynamic analyses", *Int. J. Numer. Meth. Eng.*, **32**(5), 943-955.

Hilber, H.M., Hughes, T.J. and Taylor, R.L. (1977), "Improved numerical dissipation for time integration algorithms in structural dynamics", *Earthq. Eng. Struct. Dyn.*, **5**(3), 283-292.

Hulbert, G.M. and Chung, J. (1996), "Explicit time integration algorithms for structural dynamics with optimal numerical dissipation", *Comput. Meth. Appl. Mech. Eng.* **137**(2), 175-188.

Klarmann, S. and Wagner, W. (2015), "Enhanced studies on a composite time integration scheme in linear and non-linear dynamics", *Comput. Mech.*, **55**(3), 455-468.

Kolay, C. and Ricles, J.M. (2014), "Development of a family of unconditionally stable explicit direct integration algorithms with controllable numerical energy dissipation", *Earthq. Eng. Struct. Dyn.*, **43**(9), 1361-1380.

Kuo, S.R. and Yau, J.D. (2011), "A fast and accurate step-by-step solution procedure for direct integration", *Int. J. Struct. Stab. Dyn.*, **11**(3), 473-493.

Kuo, S.R., Yau, J.D. and Yang, Y.B. (2012), "A robust time-integration algorithm for solving nonlinear dynamic problems with large rotations and displacements", *Int. J. Struct. Stab. Dyn.*, **12**(6), 1250051.

Levine, W.S. (1996), *The Control Handbook*, CRC Press.

Liu, T., Li, Q. and Zhao, C. (2013), "An efficient time-integration method for nonlinear dynamic analysis of solids and structures", *Sci. Chin.: Phys., Mechan Astron*, **56**, 798-804.

Mansur, W.J., Carrer, J.A.M., Ferreira, W.G., De Gouveia, A.C. and Venancio-Filho, F. (2000), "Time-segmented frequency-domain analysis for non-linear multi-degree-of-freedom structural systems", *J. Sound Vibr.*, **237**(3), 457-475.

Mohammadzadeh, S., Ghassemieh, M. and Park, Y. (2017), "Extended implicit integration process by utilizing nonlinear dynamics in finite element", *Struct. Eng. Mech.*, **64**(4), 495-504.

Mohammadzadeh, S., Ghassemieh, M. and Park, Y. (2017), "Structure-dependent improved Wilson-θ method with higher order of accuracy and controllable amplitude decay", *Appl. Math. Modell.*, **52**, 417-436.

Nguyen, T.L., Sansour, C. and Hjiaj, M. (2017), "Long-term stable time integration scheme for dynamic analysis of planar geometrically exact Timoshenko beams", *J. Sound Vibr.*, **396**, 144-171.

Park, K.C. (1977), "Practical aspects of numerical time integration", *Comput. Struct.*, **7**(3), 343-353.

Paz, M. and Leigh, W. (1985), *Structural Dynamics*.

Pezeshk, S. and Camp, C.V. (1995), "An explicit time-integration method for damped structural systems", *Struct. Eng. Mech.*, **3**(2), 145-162.

Razavi, S.H., Abolmaali, A. and Ghassemieh, M. (2007), "A weighted residual parabolic acceleration time integration method for problems in structural dynamics", *Comput. Meth. Appl. Math.*, **7**(3), 227-238.

Rezaiee-Pajand, M. and Alamatian, J. (2008), "Numerical time integration for dynamic analysis using a new higher order predictor-corrector method", *Eng. Comput.*, **25**(6), 541-568.

Rezaiee-Pajand, M. and Estiri, H. (2016), "Computing the structural buckling limit load by using dynamic relaxation method", *Int. J. Non-Lin. Mech.*, **81**, 245-260.

Rezaiee-Pajand, M. and Hashemian, M. (2016), "Time integration method based on discrete transfer function", *Int. J. Struct. Stab. Dyn.*, **16**(5), 1550009.

Rezaiee-Pajand, M. and Hashemian, M. (2017), "Modified differential transformation method for solving nonlinear dynamic problems", *Appl. Math. Modell.*, **47**, 76-95.

Rezaiee-Pajand, M. and Karimi-Rad, M. (2015), "More accurate and stable time integration scheme", *Eng. Comput.*, **31**(4), 791-812.

Rezaiee-Pajand, M. and Karimi-Rad, M. (2016), "A new explicit time integration scheme for nonlinear dynamic analysis", *Int. J. Struct. Stab. Dyn.*, **16**(9), 1550054.

Rezaiee-Pajand, M. and Karimi-Rad, M. (2017), "A family of second-order fully explicit time integration schemes", *Comput. Appl. Math.*

Rezaiee-Pajand, M. and Karimi-Rad, M. (2017), "An accurate predictor-corrector time integration method for structural dynamics", *Int. J. Steel Struct.*, **17**(3), 1033-1047.

Rezaiee-Pajand, M. and Sarafrazi, S.R. (2010), "A mixed and multi-step higher-order implicit time integration family", *J. Mech. Eng. Sci.*, **224**(10), 2097-2108.

Rezaiee-Pajand, M., Hashemian, M. and Bohluly, A. (2017), "A novel time integration formulation for nonlinear dynamic analysis", *Aerosp. Sci. Technol.*, **69**, 625-635.

Rio, G., Soive, A. and Grolleau, V. (2005), "Comparative study of numerical explicit time integration algorithms", *Adv. Eng. Softw.*, **36**(4), 252-265.

Saka, M.P. (1990), "Optimum design of pin-jointed steel structures with practical applications", *J. Struct. Eng.*, **116**(10), 2599-2620.

Shishvan, S.S., Noorzad, A. and Ansari, A. (2009), "A time integration algorithm for linear transient analysis based on the reproducing kernel method", *Comput. Meth. Appl. Mech. Eng.*, **198**(41), 3361-3377.

Subbaraj, K. and Dokainish, M.A. (1989), "A survey of direct time-integration methods in computational structural dynamics-II. Implicit methods", *Comput. Struct.*, **32**(6), 1387-1401.

Tang, Y. and Lou, M. (2017), " New unconditionally stable explicit integration algorithm for real-time hybrid testing", *J. Eng. Mech.*, **143**(7), 04017029.

Torkamani, M.A. and Shieh, J.H. (2011), "Higher-order stiffness matrices in nonlinear finite element analysis of plane truss structures", *Eng. Struct.*, **33**(12), 3516-3526.

Turyn, L. (2013), *Advanced Engineering Mathematics*, CRC Press.

Verma, M., Rajasankar, J. and Iyer, N.R. (2015), "Numerical assessment of step-by-step integration methods in the paradigm of real-time hybrid testing", *Earthq. Struct.*, **8**(6), 1325-1348.

Wang, M. and Au, F.T.K. (2008), "Precise integration methods based on the Chebyshev polynomial of the first kind", *Earthq. Eng. Eng. Vibr.*, **7**(2), 207-216.

Wang, M.F. and Au, F.T.K. (2009), "On the precise integration methods based on Padé approximations", *Comput. Struct.*, **87**(5), 380-390.

Wen, W.B., Jian, K.L. and Luo, S.M. (2014), "An explicit time integration method for structural dynamics using septuple B-spline functions", *Int. J. Numer. Meth. Eng.*, **97**(9), 629-657.

Wen, W.B., Wei, K., Lei, H.S., Duan, S.Y. and Fang, D.N. (2017), "A novel sub-step composite implicit time integration scheme for structural dynamics", *Comput. Struct.*, **182**, 176-186.

Wu, B., Xu, G., Wang, Q. and Williams, M.S. (2006), "Operator-splitting method for real-time substructure testing", *Earthq. Eng. Struct. Dyn.*, **35**(3), 293-314.

Yin, S.H. (2013), "A new explicit time integration method for structural dynamics", *Int. J. Struct. Stab. Dyn.*, **13**(3), 1250068.

Zhai, W.M. (1996), "Two simple fast integration methods for large-scale dynamic problems in engineering", *Int. J. Numer. Meth. Eng.*, **39**(24), 4199-4214.

Zheng, M., Yuan, Z., Tong, Q., Zhang, G. and Zhu, W. (2017), "A novel unconditionally stable explicit integration method for finite element method", *Vis. Comput.*, 1-13.

CC

Appendix A

The amplification matrix and its related coefficients for the proposed method with m=2 have the following forms

$$
\begin{aligned}
&\left[\mathbf{A}_{(2)}\right]=\begin{bmatrix} A_{(2)11} & A_{(2)12} \\ A_{(2)21} & A_{(2)22} \end{bmatrix} \\
&A_{(2)11}=1-\frac{1}{2}\omega^2\Delta t^2+\frac{1}{3}\xi\omega^3\Delta t^3+\frac{1}{24}(1-4\xi^2)\omega^4\Delta t^4+O(\Delta t^5) \\
&A_{(2)12}=\Delta t-\xi\omega\Delta t^2-\frac{1}{6}(1-4\xi^2)\omega^2\Delta t^3-\frac{1}{6}(2\xi^3-\xi)\omega^3\Delta t^4+O(\Delta t^5) \\
&A_{(2)21}=-\omega^2\Delta t+\xi\omega^3\Delta t^2+\frac{1}{6}(1-4\xi^2)\omega^4\Delta t^3+\frac{1}{24}(\frac{112}{15}\xi^3-\frac{56}{15}\xi)\omega^5\Delta t^4+O(\Delta t^5) \\
&A_{(2)22}=1-2\xi\omega\Delta t-\frac{1}{2}(1-4\xi^2)\omega^2\Delta t^2-\frac{2}{3}(2\xi^3-\xi)\omega^3\Delta t^3+\frac{1}{24}(\frac{224}{15}\xi^4-\frac{56}{5}\xi^2+\frac{14}{15})\omega^4\Delta t^4+O(\Delta t^5)
\end{aligned}
\tag{A1}
$$

The amplification matrix for m=3 can be expressed as

$$
\begin{aligned}
&\left[A_{(3)}\right]=\begin{bmatrix} A_{(3)11} & A_{(3)12} \\ A_{(3)21} & A_{(3)22} \end{bmatrix} \\
&A_{(3)11}=1-\frac{1}{2}\omega^2\Delta t^2+\frac{1}{3}\xi\omega^3\Delta t^3+\frac{1}{24}(1-4\xi^2)\omega^4\Delta t^4+\frac{1}{30}(2\xi^3-\xi)\omega^5\Delta t^5+O(\Delta t^6) \\
&A_{(3)12}=\Delta t-\xi\omega\Delta t^2-\frac{1}{6}(1-4\xi^2)\omega^2\Delta t^3-\frac{1}{6}(2\xi^3-\xi)\omega^3\Delta t^4+\frac{1}{120}(16\xi^4-12\xi^2+1)\omega^4\Delta t^5+O(\Delta t^6) \\
&A_{(3)21}=-\omega^2\Delta t+\xi\omega^3\Delta t^2+\frac{1}{6}(1-4\xi^2)\omega^4\Delta t^3+\frac{1}{6}(2\xi^3-\xi)\omega^5\Delta t^4-\frac{1}{120}(\frac{340}{21}\xi^4-\frac{85}{7}\xi^2+\frac{85}{84})\omega^6\Delta t^5+O(\Delta t^6) \\
&A_{(3)22}=1-2\xi\omega\Delta t-\frac{1}{2}(1-4\xi^2)\omega^2\Delta t^2-\frac{2}{3}(2\xi^3-\xi)\omega^3\Delta t^3+\frac{1}{24}(16\xi^4-12\xi^2+1)\omega^4\Delta t^4+\ldots \\
&-\frac{1}{120}(\frac{680}{21}\xi^5-\frac{680}{21}\xi^3+\frac{85}{14}\xi)\omega^5\Delta t^5+O(\Delta t^6)
\end{aligned}
\tag{A2}
$$

For m=4, the amplification matrix of the proposed method is

$$
\begin{aligned}
&\left[A_{(4)}\right]=\begin{bmatrix} A_{(4)11} & A_{(4)12} \\ A_{(4)21} & A_{(4)22} \end{bmatrix} \\
&A_{(4)11}=1-\frac{1}{2}\omega^2\Delta t^2+\frac{1}{3}\xi\omega^3\Delta t^3+\frac{1}{24}(1-4\xi^2)\omega^4\Delta t^4+\frac{1}{30}(2\xi^3-\xi)\omega^5\Delta t^5+\ldots \\
&-\frac{1}{720}(16\xi^4-12\xi^2+1)\omega^6\Delta t^6+O(\Delta t^7) \\
&A_{(4)12}=\Delta t-\xi\omega\Delta t^2-\frac{1}{6}(1-4\xi^2)\omega^2\Delta t^3-\frac{1}{6}(2\xi^3-\xi)\omega^3\Delta t^4+\frac{1}{120}(16\xi^4-12\xi^2+1)\omega^4\Delta t^5+\ldots \\
&-\frac{1}{720}(32\xi^5-32\xi^3+6\xi)\omega^5\Delta t^6+O(\Delta t^7) \\
&A_{(4)21}=-\omega^2\Delta t+\xi\omega^3\Delta t^2+\frac{1}{6}(1-4\xi^2)\omega^4\Delta t^3+\frac{1}{6}(2\xi^3-\xi)\omega^5\Delta t^4-\frac{1}{120}(16\xi^4-12\xi^2+1)\omega^6\Delta t^5+\ldots \\
&+\frac{1}{720}(\frac{3352}{105}\xi^5-\frac{3352}{105}\xi^3+\frac{419}{70}\xi)\omega^7\Delta t^6+O(\Delta t^7) \\
&A_{(4)22}=1-2\xi\omega\Delta t-\frac{1}{2}(1-4\xi^2)\omega^2\Delta t^2-\frac{2}{3}(2\xi^3-\xi)\omega^3\Delta t^3+\frac{1}{24}(16\xi^4-12\xi^2+1)\omega^4\Delta t^4+\ldots \\
&-\frac{1}{120}(32\xi^5-32\xi^3+6\xi)\omega^5\Delta t^5+\frac{1}{720}(\frac{6704}{105}\xi^6-\frac{1676}{21}\xi^4+\frac{838}{35}\xi^2-\frac{419}{420})\omega^6\Delta t^6+O(\Delta t^7)
\end{aligned}
\tag{A3}
$$

The analytical amplification matrix and its related coefficients are given by

$$
\begin{aligned}
&\left[A^a\right]=\begin{bmatrix} A^a_{11} & A^a_{12} \\ A^a_{21} & A^a_{22} \end{bmatrix} \\
&A^a_{11}=1-\frac{1}{2}\omega^2\Delta t^2+\frac{1}{3}\xi\omega^3\Delta t^3+\frac{1}{24}(1-4\xi^2)\omega^4\Delta t^4+\frac{1}{30}(2\xi^3-\xi)\omega^5\Delta t^5+\ldots \\
&-\frac{1}{720}(16\xi^4-12\xi^2+1)\omega^6\Delta t^6+\frac{1}{5040}(32\xi^5-32\xi^3+6\xi)\omega^7\Delta t^7+O(\Delta t^8) \\
&A^a_{12}=\Delta t-\xi\omega\Delta t^2-\frac{1}{6}(1-4\xi^2)\omega^2\Delta t^3-\frac{1}{6}(2\xi^3-\xi)\omega^3\Delta t^4+\frac{1}{120}(16\xi^4-12\xi^2+1)\omega^4\Delta t^5+\ldots \\
&-\frac{1}{720}(32\xi^5-32\xi^3+6\xi)\omega^5\Delta t^6+\frac{1}{5040}(64\xi^6-80\xi^4+24\xi^2-1)\omega^6\Delta t^7+O(\Delta t^8) \\
&A^a_{21}=-\omega^2\Delta t+\xi\omega^3\Delta t^2+\frac{1}{6}(1-4\xi^2)\omega^4\Delta t^3+\frac{1}{6}(2\xi^3-\xi)\omega^5\Delta t^4-\frac{1}{120}(16\xi^4-12\xi^2+1)\omega^6\Delta t^5+\ldots \\
&+\frac{1}{720}(32\xi^5-32\xi^3+6\xi)\omega^7\Delta t^6-\frac{1}{5040}(64\xi^6-80\xi^4+24\xi^2-1)\omega^8\Delta t^7+O(\Delta t^8) \\
&A^a_{22}=1-2\xi\omega\Delta t-\frac{1}{2}(1-4\xi^2)\omega^2\Delta t^2-\frac{2}{3}(2\xi^3-\xi)\omega^3\Delta t^3+\frac{1}{24}(16\xi^4-12\xi^2+1)\omega^4\Delta t^4-\frac{1}{120}(32\xi^5-32\xi^3+6\xi)\omega^5\Delta t^5+\ldots \\
&+\frac{1}{720}(64\xi^6-80\xi^4+24\xi^2-1)\omega^6\Delta t^6-\frac{1}{5040}(128\xi^7-192\xi^5+80\xi^3-8\xi)\omega^7\Delta t^7+O(\Delta t^8)
\end{aligned}
\tag{A4}
$$